Fermilab-Pub-11-288-E

Search for Higgs bosons decaying to $\tau^+\tau^-$ pairs in $p\overline{p}$ collisions at $\sqrt{s} = 1.96$ TeV

V.M. Abazov,[35] B. Abbott,[73] B.S. Acharya,[29] M. Adams,[49] T. Adams,[47] G.D. Alexeev,[35] G. Alkhazov,[39] A. Alton[a],[61] G. Alverson,[60] G.A. Alves,[2] M. Aoki,[48] M. Arov,[58] A. Askew,[47] B. Åsman,[41] O. Atramentov,[65] C. Avila,[8] J. BackusMayes,[80] F. Badaud,[13] L. Bagby,[48] B. Baldin,[48] D.V. Bandurin,[47] S. Banerjee,[29] E. Barberis,[60] P. Baringer,[56] J. Barreto,[3] J.F. Bartlett,[48] U. Bassler,[18] V. Bazterra,[49] S. Beale,[6] A. Bean,[56] M. Begalli,[3] M. Begel,[71] C. Belanger-Champagne,[41] L. Bellantoni,[48] S.B. Beri,[27] G. Bernardi,[17] R. Bernhard,[22] I. Bertram,[42] M. Besançon,[18] R. Beuselinck,[43] V.A. Bezzubov,[38] P.C. Bhat,[48] V. Bhatnagar,[27] G. Blazey,[50] S. Blessing,[47] K. Bloom,[64] A. Boehnlein,[48] D. Boline,[70] E.E. Boos,[37] G. Borissov,[42] T. Bose,[59] A. Brandt,[76] O. Brandt,[23] R. Brock,[62] G. Brooijmans,[68] A. Bross,[48] D. Brown,[17] J. Brown,[17] X.B. Bu,[48] M. Buehler,[79] V. Buescher,[24] V. Bunichev,[37] S. Burdin[b],[42] T.H. Burnett,[80] C.P. Buszello,[41] B. Calpas,[15] E. Camacho-Pérez,[32] M.A. Carrasco-Lizarraga,[56] B.C.K. Casey,[48] H. Castilla-Valdez,[32] S. Chakrabarti,[70] D. Chakraborty,[50] K.M. Chan,[54] A. Chandra,[78] G. Chen,[56] S. Chevalier-Théry,[18] D.K. Cho,[75] S.W. Cho,[31] S. Choi,[31] B. Choudhary,[28] S. Cihangir,[48] D. Claes,[64] J. Clutter,[56] M. Cooke,[48] W.E. Cooper,[48] M. Corcoran,[78] F. Couderc,[18] M.-C. Cousinou,[15] A. Croc,[18] D. Cutts,[75] A. Das,[45] G. Davies,[43] K. De,[76] S.J. de Jong,[34] E. De La Cruz-Burelo,[32] F. Déliot,[18] M. Demarteau,[48] R. Demina,[69] D. Denisov,[48] S.P. Denisov,[38] S. Desai,[48] C. Deterre,[18] K. DeVaughan,[64] H.T. Diehl,[48] M. Diesburg,[48] P.F. Ding,[44] A. Dominguez,[64] T. Dorland,[80] A. Dubey,[28] L.V. Dudko,[37] D. Duggan,[65] A. Duperrin,[15] S. Dutt,[27] A. Dyshkant,[50] M. Eads,[64] D. Edmunds,[62] J. Ellison,[46] V.D. Elvira,[48] Y. Enari,[17] H. Evans,[52] A. Evdokimov,[71] V.N. Evdokimov,[38] G. Facini,[60] T. Ferbel,[69] F. Fiedler,[24] F. Filthaut,[34] W. Fisher,[62] H.E. Fisk,[48] M. Fortner,[50] H. Fox,[42] S. Fuess,[48] A. Garcia-Bellido,[69] V. Gavrilov,[36] P. Gay,[13] W. Geng,[15,62] D. Gerbaudo,[66] C.E. Gerber,[49] Y. Gershtein,[65] G. Ginther,[48,69] G. Golovanov,[35] A. Goussiou,[80] P.D. Grannis,[70] S. Greder,[19] H. Greenlee,[48] Z.D. Greenwood,[58] E.M. Gregores,[4] G. Grenier,[20] Ph. Gris,[13] J.-F. Grivaz,[16] A. Grohsjean,[18] S. Grünendahl,[48] M.W. Grünewald,[30] T. Guillemin,[16] F. Guo,[70] G. Gutierrez,[48] P. Gutierrez,[73] A. Haas[c],[68] S. Hagopian,[47] J. Haley,[60] L. Han,[7] K. Harder,[44] A. Harel,[69] J.M. Hauptman,[55] J. Hays,[43] T. Head,[44] T. Hebbeker,[21] D. Hedin,[50] H. Hegab,[74] A.P. Heinson,[46] U. Heintz,[75] C. Hensel,[23] I. Heredia-De La Cruz,[32] K. Herner,[61] G. Hesketh[d],[44] M.D. Hildreth,[54] R. Hirosky,[79] T. Hoang,[47] J.D. Hobbs,[70] B. Hoeneisen,[12] M. Hohlfeld,[24] Z. Hubacek,[10,18] N. Huske,[17] V. Hynek,[10] I. Iashvili,[67] Y. Ilchenko,[77] R. Illingworth,[48] A.S. Ito,[48] S. Jabeen,[75] M. Jaffré,[16] D. Jamin,[15] A. Jayasinghe,[73] R. Jesik,[43] K. Johns,[45] M. Johnson,[48] D. Johnston,[64] A. Jonckheere,[48] P. Jonsson,[43] J. Joshi,[27] A.W. Jung,[48] A. Juste,[40] K. Kaadze,[57] E. Kajfasz,[15] D. Karmanov,[37] P.A. Kasper,[48] I. Katsanos,[64] R. Kehoe,[77] S. Kermiche,[15] N. Khalatyan,[48] A. Khanov,[74] A. Kharchilava,[67] Y.N. Kharzheev,[35] M.H. Kirby,[51] J.M. Kohli,[27] A.V. Kozelov,[38] J. Kraus,[62] S. Kulikov,[38] A. Kumar,[67] A. Kupco,[11] T. Kurča,[20] V.A. Kuzmin,[37] J. Kvita,[9] S. Lammers,[52] G. Landsberg,[75] P. Lebrun,[20] H.S. Lee,[31] S.W. Lee,[55] W.M. Lee,[48] J. Lellouch,[17] L. Li,[46] Q.Z. Li,[48] S.M. Lietti,[5] J.K. Lim,[31] D. Lincoln,[48] J. Linnemann,[62] V.V. Lipaev,[38] R. Lipton,[48] Y. Liu,[7] Z. Liu,[6] A. Lobodenko,[39] M. Lokajicek,[11] R. Lopes de Sa,[70] H.J. Lubatti,[80] R. Luna-Garcia[e],[32] A.L. Lyon,[48] A.K.A. Maciel,[2] D. Mackin,[78] R. Madar,[18] R. Magaña-Villalba,[32] S. Malik,[64] V.L. Malyshev,[35] Y. Maravin,[57] J. Martínez-Ortega,[32] R. McCarthy,[70] C.L. McGivern,[56] M.M. Meijer,[34] A. Melnitchouk,[63] D. Menezes,[50] P.G. Mercadante,[4] M. Merkin,[37] A. Meyer,[21] J. Meyer,[23] F. Miconi,[19] N.K. Mondal,[29] G.S. Muanza,[15] M. Mulhearn,[79] E. Nagy,[15] M. Naimuddin,[28] M. Narain,[75] R. Nayyar,[28] H.A. Neal,[61] J.P. Negret,[8] P. Neustroev,[39] S.F. Novaes,[5] T. Nunnemann,[25] G. Obrant[‡],[39] J. Orduna,[78] N. Osman,[15] J. Osta,[54] G.J. Otero y Garzón,[1] M. Padilla,[46] A. Pal,[76] N. Parashar,[53] V. Parihar,[75] S.K. Park,[31] J. Parsons,[68] R. Partridge[c],[75] N. Parua,[52] A. Patwa,[71] B. Penning,[48] M. Perfilov,[37] K. Peters,[44] Y. Peters,[44] K. Petridis,[44] G. Petrillo,[69] P. Pétroff,[16] R. Piegaia,[1] M.-A. Pleier,[71] P.L.M. Podesta-Lerma[f],[32] V.M. Podstavkov,[48] P. Polozov,[36] A.V. Popov,[38] M. Prewitt,[78] D. Price,[52] N. Prokopenko,[38] S. Protopopescu,[71] J. Qian,[61] A. Quadt,[23] B. Quinn,[63] M.S. Rangel,[2] K. Ranjan,[28] P.N. Ratoff,[42] I. Razumov,[38] P. Renkel,[77] M. Rijssenbeek,[70] I. Ripp-Baudot,[19] F. Rizatdinova,[74] M. Rominsky,[48] A. Ross,[42] C. Royon,[18] P. Rubinov,[48] R. Ruchti,[54] G. Safronov,[36] G. Sajot,[14] P. Salcido,[50] A. Sánchez-Hernández,[32] M.P. Sanders,[25] B. Sanghi,[48] A.S. Santos,[5] G. Savage,[48] L. Sawyer,[58] T. Scanlon,[43] R.D. Schamberger,[70] Y. Scheglov,[39] H. Schellman,[51] T. Schliephake,[26] S. Schlobohm,[80] C. Schwanenberger,[44] R. Schwienhorst,[62] J. Sekaric,[56] H. Severini,[73] E. Shabalina,[23] V. Shary,[18] A.A. Shchukin,[38] R.K. Shivpuri,[28] V. Simak,[10] V. Sirotenko,[48] P. Skubic,[73] P. Slattery,[69] D. Smirnov,[54] K.J. Smith,[67] G.R. Snow,[64]

J. Snow,[72] S. Snyder,[71] S. Söldner-Rembold,[44] L. Sonnenschein,[21] K. Soustruznik,[9] J. Stark,[14] V. Stolin,[36] D.A. Stoyanova,[38] M. Strauss,[73] D. Strom,[49] L. Stutte,[48] L. Suter,[44] P. Svoisky,[73] M. Takahashi,[44] A. Tanasijczuk,[1] W. Taylor,[6] M. Titov,[18] V.V. Tokmenin,[35] Y.-T. Tsai,[69] D. Tsybychev,[70] B. Tuchming,[18] C. Tully,[66] L. Uvarov,[39] S. Uvarov,[39] S. Uzunyan,[50] R. Van Kooten,[52] W.M. van Leeuwen,[33] N. Varelas,[49] E.W. Varnes,[45] I.A. Vasilyev,[38] P. Verdier,[20] L.S. Vertogradov,[35] M. Verzocchi,[48] M. Vesterinen,[44] D. Vilanova,[18] P. Vokac,[10] H.D. Wahl,[47] M.H.L.S. Wang,[48] J. Warchol,[54] G. Watts,[80] M. Wayne,[54] M. Weber[g],[48] L. Welty-Rieger,[51] A. White,[76] D. Wicke,[26] M.R.J. Williams,[42] G.W. Wilson,[56] M. Wobisch,[58] D.R. Wood,[60] T.R. Wyatt,[44] Y. Xie,[48] C. Xu,[61] S. Yacoob,[51] R. Yamada,[48] W.-C. Yang,[44] T. Yasuda,[48] Y.A. Yatsunenko,[35] Z. Ye,[48] H. Yin,[48] K. Yip,[71] S.W. Youn,[48] J. Yu,[76] S. Zelitch,[79] T. Zhao,[80] B. Zhou,[61] J. Zhu,[61] M. Zielinski,[69] D. Zieminska,[52] and L. Zivkovic[75]

(The D0 Collaboration*)

[1]*Universidad de Buenos Aires, Buenos Aires, Argentina*
[2]*LAFEX, Centro Brasileiro de Pesquisas Físicas, Rio de Janeiro, Brazil*
[3]*Universidade do Estado do Rio de Janeiro, Rio de Janeiro, Brazil*
[4]*Universidade Federal do ABC, Santo André, Brazil*
[5]*Instituto de Física Teórica, Universidade Estadual Paulista, São Paulo, Brazil*
[6]*Simon Fraser University, Vancouver, British Columbia, and York University, Toronto, Ontario, Canada*
[7]*University of Science and Technology of China, Hefei, People's Republic of China*
[8]*Universidad de los Andes, Bogotá, Colombia*
[9]*Charles University, Faculty of Mathematics and Physics, Center for Particle Physics, Prague, Czech Republic*
[10]*Czech Technical University in Prague, Prague, Czech Republic*
[11]*Center for Particle Physics, Institute of Physics, Academy of Sciences of the Czech Republic, Prague, Czech Republic*
[12]*Universidad San Francisco de Quito, Quito, Ecuador*
[13]*LPC, Université Blaise Pascal, CNRS/IN2P3, Clermont, France*
[14]*LPSC, Université Joseph Fourier Grenoble 1, CNRS/IN2P3, Institut National Polytechnique de Grenoble, Grenoble, France*
[15]*CPPM, Aix-Marseille Université, CNRS/IN2P3, Marseille, France*
[16]*LAL, Université Paris-Sud, CNRS/IN2P3, Orsay, France*
[17]*LPNHE, Universités Paris VI and VII, CNRS/IN2P3, Paris, France*
[18]*CEA, Irfu, SPP, Saclay, France*
[19]*IPHC, Université de Strasbourg, CNRS/IN2P3, Strasbourg, France*
[20]*IPNL, Université Lyon 1, CNRS/IN2P3, Villeurbanne, France and Université de Lyon, Lyon, France*
[21]*III. Physikalisches Institut A, RWTH Aachen University, Aachen, Germany*
[22]*Physikalisches Institut, Universität Freiburg, Freiburg, Germany*
[23]*II. Physikalisches Institut, Georg-August-Universität Göttingen, Göttingen, Germany*
[24]*Institut für Physik, Universität Mainz, Mainz, Germany*
[25]*Ludwig-Maximilians-Universität München, München, Germany*
[26]*Fachbereich Physik, Bergische Universität Wuppertal, Wuppertal, Germany*
[27]*Panjab University, Chandigarh, India*
[28]*Delhi University, Delhi, India*
[29]*Tata Institute of Fundamental Research, Mumbai, India*
[30]*University College Dublin, Dublin, Ireland*
[31]*Korea Detector Laboratory, Korea University, Seoul, Korea*
[32]*CINVESTAV, Mexico City, Mexico*
[33]*Nikhef, Science Park, Amsterdam, the Netherlands*
[34]*Radboud University Nijmegen, Nijmegen, the Netherlands and Nikhef, Science Park, Amsterdam, the Netherlands*
[35]*Joint Institute for Nuclear Research, Dubna, Russia*
[36]*Institute for Theoretical and Experimental Physics, Moscow, Russia*
[37]*Moscow State University, Moscow, Russia*
[38]*Institute for High Energy Physics, Protvino, Russia*
[39]*Petersburg Nuclear Physics Institute, St. Petersburg, Russia*
[40]*Institució Catalana de Recerca i Estudis Avançats (ICREA) and Institut de Física d'Altes Energies (IFAE), Barcelona, Spain*
[41]*Stockholm University, Stockholm and Uppsala University, Uppsala, Sweden*
[42]*Lancaster University, Lancaster LA1 4YB, United Kingdom*
[43]*Imperial College London, London SW7 2AZ, United Kingdom*
[44]*The University of Manchester, Manchester M13 9PL, United Kingdom*
[45]*University of Arizona, Tucson, Arizona 85721, USA*
[46]*University of California Riverside, Riverside, California 92521, USA*
[47]*Florida State University, Tallahassee, Florida 32306, USA*
[48]*Fermi National Accelerator Laboratory, Batavia, Illinois 60510, USA*

[49]University of Illinois at Chicago, Chicago, Illinois 60607, USA
[50]Northern Illinois University, DeKalb, Illinois 60115, USA
[51]Northwestern University, Evanston, Illinois 60208, USA
[52]Indiana University, Bloomington, Indiana 47405, USA
[53]Purdue University Calumet, Hammond, Indiana 46323, USA
[54]University of Notre Dame, Notre Dame, Indiana 46556, USA
[55]Iowa State University, Ames, Iowa 50011, USA
[56]University of Kansas, Lawrence, Kansas 66045, USA
[57]Kansas State University, Manhattan, Kansas 66506, USA
[58]Louisiana Tech University, Ruston, Louisiana 71272, USA
[59]Boston University, Boston, Massachusetts 02215, USA
[60]Northeastern University, Boston, Massachusetts 02115, USA
[61]University of Michigan, Ann Arbor, Michigan 48109, USA
[62]Michigan State University, East Lansing, Michigan 48824, USA
[63]University of Mississippi, University, Mississippi 38677, USA
[64]University of Nebraska, Lincoln, Nebraska 68588, USA
[65]Rutgers University, Piscataway, New Jersey 08855, USA
[66]Princeton University, Princeton, New Jersey 08544, USA
[67]State University of New York, Buffalo, New York 14260, USA
[68]Columbia University, New York, New York 10027, USA
[69]University of Rochester, Rochester, New York 14627, USA
[70]State University of New York, Stony Brook, New York 11794, USA
[71]Brookhaven National Laboratory, Upton, New York 11973, USA
[72]Langston University, Langston, Oklahoma 73050, USA
[73]University of Oklahoma, Norman, Oklahoma 73019, USA
[74]Oklahoma State University, Stillwater, Oklahoma 74078, USA
[75]Brown University, Providence, Rhode Island 02912, USA
[76]University of Texas, Arlington, Texas 76019, USA
[77]Southern Methodist University, Dallas, Texas 75275, USA
[78]Rice University, Houston, Texas 77005, USA
[79]University of Virginia, Charlottesville, Virginia 22901, USA
[80]University of Washington, Seattle, Washington 98195, USA

(Dated: June 24, 2011)

We present a search for the production of neutral Higgs bosons decaying into $\tau^+\tau^-$ pairs in $p\bar{p}$ collisions at a center-of-mass energy of 1.96 TeV. The data, corresponding to an integrated luminosity of 5.4 fb^{-1}, were collected by the D0 experiment at the Fermilab Tevatron Collider. We set upper limits at the 95% C.L. on the production cross section multiplied by the branching ratio for a scalar resonance decaying into $\tau^+\tau^-$ pairs, and we then interpret these limits as limits on the production of Higgs bosons in the minimal supersymmetric standard model (MSSM) and as constraints in the MSSM parameter space.

PACS numbers: 14.80.Ec,14.80.Da,13.85.Rm

Supersymmetry (SUSY) [1] is one of the extensions of the standard model (SM) proposed to address its shortcomings, such as the hierarchy problem caused by the divergent radiative corrections to the Higgs boson mass. In the minimal supersymmetric standard model (MSSM), two complex Higgs boson doublets lead to five physical Higgs bosons: two neutral CP-even (h, H), one neutral CP-odd (A), and two charged Higgs bosons ($H^{\pm}$). The three neutral Higgs bosons (h, H, A) are collectively denoted as ϕ. At tree level, the Higgs sector of the MSSM is fully described by two parameters, which are commonly chosen to be the mass of the CP-odd Higgs boson, M_A, and the ratio of the vacuum expectation values of the two Higgs doublets, $\tan\beta$. Radiative corrections introduce dependencies on additional MSSM parameters. The neutral MSSM Higgs bosons decay into $\tau^+\tau^-$ and $b\bar{b}$ pairs with branching fractions of $\approx 10\%$ and $\approx 90\%$, respectively. Their production cross section is enhanced by a factor that depends on $\tan\beta$ with respect to the cross section for the SM Higgs boson at the same Higgs boson mass. Moreover, for large $\tan\beta$, the Higgs bosons A and either h or H are nearly degenerate in mass which leads to an approximate doubling of $\sigma_\phi(M_\phi)$.

Searches for the production of neutral MSSM Higgs bosons have been performed at the CERN e^+e^- Collider (LEP), excluding $M_{h,A} < 93$ GeV for all $\tan\beta$ [2].

*with visitors from [a]Augustana College, Sioux Falls, SD, USA, [b]The University of Liverpool, Liverpool, UK, [c]SLAC, Menlo Park, CA, USA, [d]University College London, London, UK, [e]Centro de Investigacion en Computacion - IPN, Mexico City, Mexico, [f]ECFM, Universidad Autonoma de Sinaloa, Culiacán, Mexico, and [g]Universität Bern, Bern, Switzerland. ‡Deceased.

The CDF and D0 Collaborations at the Fermilab Tevatron Collider and the CMS Collaboration at the CERN Large Hadron Collider have extended the exclusion to higher M_A of up to 300 GeV in a restricted region of $\tan\beta \approx 30-100$, by searching for the exclusive processes $(b)b\phi \to (b)bb\bar{b}$ [3] and $b\phi \to b\tau^+\tau^-$ [4], and for the inclusive process $\phi \to \tau^+\tau^-$ [5–8].

This Letter presents a search for the inclusive process $gg, b\bar{b} \to \phi \to \tau^+\tau^-$, where the tau lepton pairs are reconstructed through their decay into $e\mu$ or $\mu\tau_h$ final states, and τ_h represents the hadronic decay modes of the tau lepton. The search for $\tau^+\tau^-$ final states is performed in a model-independent way before the MSSM is chosen as one of the models to interpret the results. The data were recorded with the D0 detector [9] at a $p\bar{p}$ center-of-mass energy of $\sqrt{s} = 1.96$ TeV and correspond to an integrated luminosity of 5.4 fb^{-1}. This represents a significant increase compared to the results previously published by the CDF and D0 Collaborations, which are based on integrated luminosities of 1.8 fb^{-1} [7] and 1.0 fb^{-1} [8], respectively.

Signal samples are generated using the PYTHIA [10] Monte Carlo (MC) event generator with the CTEQ6L1 parton distribution functions (PDF) [11]. Dominant background processes comprise Z+jets, W+jets, and multijet production. Background from multijet events arises when jets are misidentified as leptons. Additional backgrounds include $t\bar{t}$ and SM diboson production. The backgrounds from Z+jets, W+jets, and $t\bar{t}$ production are modeled using ALPGEN [12], with parton showering and hadronization provided by PYTHIA. Diboson processes (WW, WZ, ZZ) are simulated using PYTHIA. In all cases TAUOLA [13] is used to model the tau lepton decays. Simulated events are then processed by a GEANT-based [14] simulation of the D0 detector, and data events from random beam crossings are overlaid to model detector noise and multiple $p\bar{p}$ interactions. Higher order quantum chromodynamics (QCD) calculations of cross sections are used to normalize the simulated background samples, except for the background from multijet production, for which the normalization and differential distributions are derived from data.

Events are selected by requiring at least one single muon trigger for the $\mu\tau_h$ channel, while for the $e\mu$ channel, they need to fulfill either inclusive electron or muon trigger conditions. Electrons are reconstructed using their characteristic energy deposits, including the transverse and longitudinal shower profiles in the electromagnetic (EM) calorimeter. Muons are identified by combining tracks in the central tracking detector with patterns of hits in the muon spectrometer. Electrons and muons are required to be isolated in the calorimeter and in the tracking detectors.

Tau lepton decays into hadrons are characterized as narrow, isolated jets with lower track multiplicity than quark or gluon jets. Three types of tau lepton decays are distinguished by their detector signature. One-prong tau decays consisting of energy deposited in the hadronic calorimeter associated with a single track ($\pi^\pm\nu$-like) are denoted as τ-type 1; τ-type 2 corresponds to one-prong tau decays with energy deposited in both the hadronic and EM calorimeters, associated with a single track ($\rho^\pm\nu$-like); and τ-type 3 are multi-prong decays with energy in the calorimeter and two or more associated tracks with invariant mass below 1.7 GeV. A calibration for the energy of τ_h candidates measured in the calorimeter is derived from data. It is based on the ratio of the calorimeter energy and the transverse momentum, p_T, measured in the tracking detector for the τ_h candidates. The ratio is adjusted in the simulation to match the data as a function of the fraction of the τ_h energy deposited in the EM calorimeter.

A set of neural networks, one for each τ-type, is applied to discriminate hadronic tau decays from jets [15]. The input variables are related to isolation and shower shapes, and exploit correlations between calorimeter energy deposits and tracks. When requiring the neural network discriminants (NN_τ) to be $NN_\tau > 0.9$ for τ-types 1, 2 and $NN_\tau > 0.95$ for τ-type 3, approximately 67% of $Z/\gamma^* \to \tau^+\tau^-$ events are retained, while 98% of the multijet background events are rejected.

A series of selections is used to reduce the background from Z+jets, W+jets, and multijet production. The $Z/\gamma^* \to \tau^-\tau^+$ process differs from a Higgs boson signal only through the mass and spin of the produced resonance and cannot be further reduced. One isolated muon with $p_T^\mu > 15$ GeV and an isolated hadronic tau lepton with transverse energy $E_T^\tau > 12.5$ GeV (τ-types 1, 2) or $E_T^\tau > 15$ GeV (τ-type 3) are required in the $\mu\tau_h$ channel. The muon and the τ_h must be oppositely charged, where the charge of the τ_h candidate is determined by the curvature of the associated track, which in case of τ-type 3 is taken to be the highest p_T track. The pseudorapidity η [16] is required to be $|\eta_\mu| < 1.6$ for muons and $|\eta_\tau| < 2.5$ for tau leptons. The transverse momentum sums of all tracks associated with the τ_h candidate, p_T^τ, are required to be greater than 7, 5, 10 GeV for τ-types 1, 2, and 3, respectively. At least one hit in the active layers of the D0 silicon vertex detector is required for the tracks associated with the τ_h. The τ_h and the muon are required to originate from the same $p\bar{p}$ vertex and must be separated from each other by $\Delta\mathcal{R} = \sqrt{(\Delta\eta)^2 + (\Delta\varphi)^2} > 0.5$, where $\Delta\varphi$ is the difference in azimuthal angle. This requirement suppresses the $Z/\gamma^* \to \mu^+\mu^-$ background. The transverse W boson mass in $W \to \ell\nu$ events is given by $M_T^{\ell\nu} = \sqrt{2p_T^\ell \not{E}_T \left[1 - \cos(\Delta\varphi(\ell, \not{E}_T)\right]}$ with $\ell = e, \mu$. The components $\not{E}_x$ and $\not{E}_y$ of the missing transverse energy, $\not{E}_T$, are computed from calorimeter cells and the momenta of muons, and corrected for the energy response of electrons, tau leptons, and jets. We require $M_T^{\mu\nu} < 50$ GeV to reject $W(\to \mu\nu)$+jets events where jets are misidentified as τ_h candidates.

In the $e\mu$ channel, events with at least one muon with $p_T^\mu > 10$ GeV and $|\eta_\mu| < 1.6$, and an oppositely charged electron with $p_T^e > 12$ GeV and $|\eta_e| < 2$ are selected. The $e\mu$ pair formed by the leptons with the highest p_T are selected as a candidate; they must be separated by $\Delta\mathcal{R} > 0.4$. To reject $Z \to \mu\mu\gamma$ events, an electron candidate is rejected if it shares the same track with a muon. Multijet background and W boson production are suppressed by requiring the mass of the $e\mu$ pair to be larger than 20 GeV and $\not\!\!E_T + p_T^\mu + p_T^e > 65$ GeV. Background from W+jets production is reduced by requiring $\min\{M_T^{e\nu}, M_T^{\mu\nu}\} < 10$ GeV. The difference in the azimuthal angle, $\Delta\varphi(\ell, \not\!\!E_T)$, has to be < 0.3 where $\ell = e, \mu$ is the lepton with the smaller p_T. This requirement rejects background from WW, $t\bar{t}$, and W+jets production. Requiring the scalar sum of the transverse momenta of all jets to be < 70 GeV rejects a large fraction of $t\bar{t}$ events.

To determine the expected background contribution from multijet production in the $\mu\tau_h$ channel, two NN_τ regions are selected in addition to the high NN_τ "signal" region defined previously: the "medium" region in the range $0.25 \leq NN_\tau \leq 0.75$ and the "low" region with $NN_\tau \leq 0.1$. The samples are further divided depending on whether the muon and the τ_h candidate have the same or opposite charge. Background from W+jets production in these samples is reduced by requiring $M_T^{\mu\nu} < 50$ GeV. The transverse mass is calculated from the missing transverse energy in the calorimeter, $\not\!\!E_T$, and from the azimuthal angle $\Delta\varphi(\mu, \not\!\!E_T)$ between the direction of the muon transverse momentum p_T^μ and the $\not\!\!E_T$. The estimated contribution from MC-simulated background processes is then subtracted from the resulting distributions, and the shape of the multijet background is derived from the distributions of same-sign $\mu\tau_h$ pairs with $NN_\tau > 0.9$. Multijet events mainly populate the low NN_τ region, and the ratio of opposite to same-sign $\mu\tau_h$ pair events in this region yields the normalization of multijet events in the signal sample. This estimate of the multijet background contribution is verified by an independent method which uses the medium NN_τ region. The difference between the estimates obtained by the two methods is used as systematic uncertainty on the multijet background.

Multijet background in the $e\mu$ channel is determined by applying the same selection criteria as for signal apart from the electron likelihood and muon isolation criteria, which are inverted. The normalization is then taken from the ratio of the numbers of events in the opposite and same-sign samples.

Since there are multiple neutrinos in the $\mu\tau_h$ and $e\mu$ final states, the $\tau^+\tau^-$ mass cannot be fully reconstructed. Therefore, we search for an enhancement above the expected background in the distribution of the visible mass $M_{\rm vis} = \sqrt{(P_{\tau_1} + P_{\tau_2} + \not\!\!P_T)^2}$, which is calculated using the four-vectors of the measured tau lepton decay products, $P_{\tau_{1,2}}$, and the missing transverse momentum,

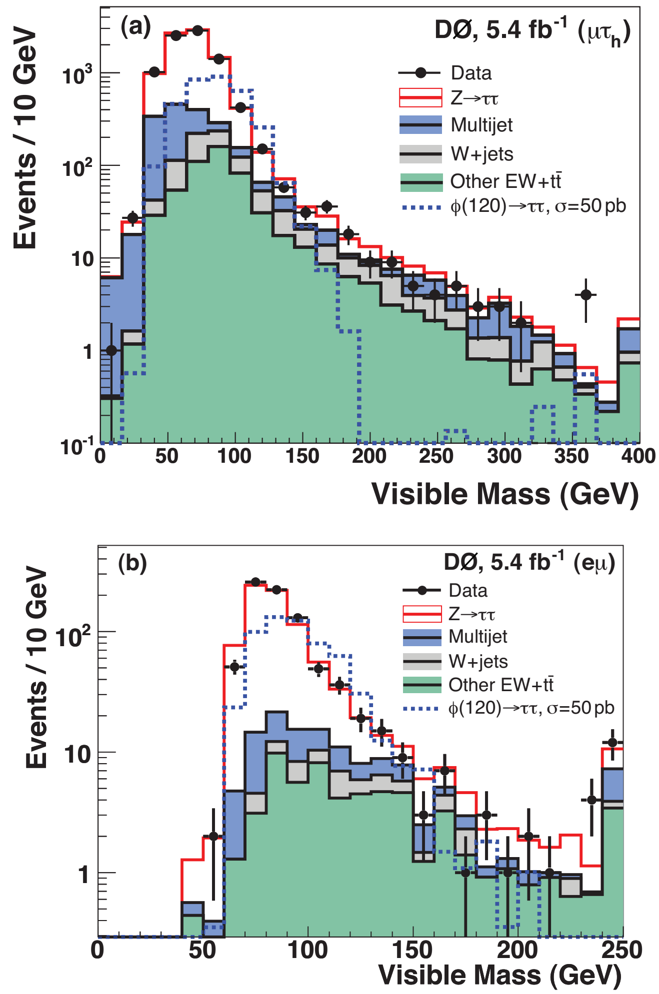

FIG. 1: Distributions of $M_{\rm vis}$ in the (a) $\mu\tau_h$ and (b) $e\mu$ channels after all selections. The data, shown with statistical uncertainties, are compared to the sum of the predicted backgrounds for an integrated luminosity of 5.4 fb^{-1}. The Higgs boson signal for $M_\phi = 120$ GeV is normalized to a production cross section of $\sigma_\phi = 50$ pb. All entries exceeding the range of a histogram are added to the last bin.

$\not\!\!P_T = (\not\!\!E_T, \not\!\!E_x, \not\!\!E_y, 0)$. In the $e\mu$ final state, the four-vectors $P_{\tau_{1,2}}$ are calculated using the reconstructed electron and muon, respectively. After imposing all selection requirements, the $M_{\rm vis}$ distributions for the $\mu\tau_h$ and $e\mu$ final states are shown in Fig. 1. Table I gives the yields of the predicted background and of data, summed over the $M_{\rm vis}$ distributions shown in Fig. 1.

Several sources of systematic uncertainty affect both the signal efficiency and background estimation. Both uncertainties that modify only the normalization and uncertainties that change the shape of the $M_{\rm vis}$ distribution are taken into account. Those that affect the normalization include the integrated luminosity (6.1%), muon identification efficiency (2.9%), τ_h identification (12%, 4.2%, 7% per τ-type), efficiency to reconstruct the τ_h track

TABLE I: Expected number of events for backgrounds, number of events observed in data and efficiency, relative to all τ lepton decays, for a signal with $M_\phi = 120$ GeV summed over the $M_{\rm vis}$ distributions shown in Fig. 1. The total uncertainties are also given.

Channel	$\mu\tau_h$	$e\mu$
$Z/\gamma^* \to \tau^+\tau^-$	6914 ± 591	697 ± 55
Multijet	972 ± 98	53 ± 8
$W \to e\nu, \mu\nu, \tau\nu$	363 ± 60	19 ± 5
$Z/\gamma^* \to e^+e^-, \mu^+\mu^-$	353 ± 32	34 ± 6
Diboson + $t\bar{t}$	180 ± 12	27 ± 5
Total Background	8782 ± 603	830 ± 56
Data	8574	825
Efficiency (%)	1.16 ± 0.03	0.20 ± 0.01

(1.4%), electron identification efficiency (3.5%), PDF uncertainty on the acceptance (4.6%), the uncertainty on the Z+jets cross sections (5%), the W+jets normalization (10% for $e\mu$ and 20% for $\mu\tau_h$), $t\bar{t}$ cross section (10%), diboson cross section (6%), muon and electron trigger efficiencies (both 5%), jet energy scale (1.5% − 2%), and the modeling of the multijet background (9.1%, 17.7%, 12.5% per τ-type). Uncertainties arising from modeling of the Z boson transverse momentum and the τ_h energy scales modify the shape of the $M_{\rm vis}$ distribution.

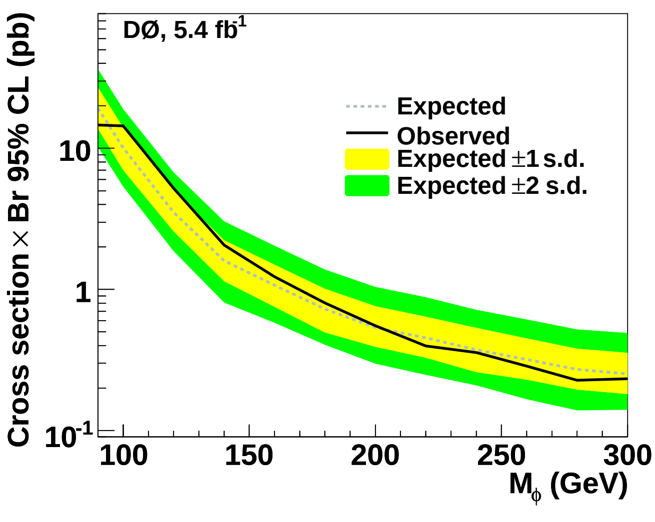

FIG. 2: Model-independent expected and observed 95% C.L. upper limits on the cross section multiplied by the branching ratio for inclusive $p\bar{p} \to \phi \to \tau^+\tau^-$ production as a function of M_ϕ, assuming a SM total width for the Higgs boson. The $\pm 1, 2$ standard deviation (s.d.) variations of the expected limits are shown as bands.

The $M_{\rm vis}$ distribution is used to calculate upper limits on the cross section based on a modified frequentist method with a Poisson log-likelihood ratio test statistics [17] and a profiling technique to reduce the impact of systematic uncertainties [18]. The confidence level, CL_s, is defined as $CL_s = CL_{s+b}/CL_b$, where CL_{s+b} and CL_b are the confidence levels in the signal+background and background-only hypotheses, respectively. The combined limits on the production cross section multiplied by the branching fraction into tau lepton pairs are given in Fig. 2 and Table II as a function of M_ϕ. The combined limits assume a scalar resonance with the decay width of a SM Higgs boson, which is negligible compared to the experimental resolution on $M_{\rm vis}$.

TABLE II: Upper limits on the expected and observed cross section (in pb) multiplied by the branching ratio for $\phi \to \tau^+\tau^-$ at the 95% C.L. as a function of M_ϕ (in GeV).

M_ϕ	Observed	−1 s.d.	Expected	+1 s.d.
90	14.7	13.8	19.2	27.1
100	14.4	7.00	10.1	14.0
120	5.22	2.58	3.53	5.01
140	2.06	1.14	1.60	2.23
160	1.23	0.75	1.07	1.50
180	0.80	0.50	0.73	1.01
200	0.55	0.39	0.54	0.76
220	0.40	0.33	0.45	0.64
240	0.36	0.26	0.37	0.53
260	0.29	0.23	0.32	0.45
280	0.23	0.19	0.27	0.38
300	0.23	0.18	0.25	0.36

In addition to M_A and $\tan\beta$, the masses and couplings of the Higgs bosons in the MSSM depend on additional parameters through radiative corrections. The production cross section limits are therefore translated into exclusions in the tanβ versus M_A plane for two representative MSSM scenarios assuming a CP-conserving Higgs sector [19], the $m_h^{\rm max}$ scenario [20] and the no-mixing scenario [21] with a Higgs mass parameter $\mu = +200$ GeV. The signal cross sections, widths, and branching ratios are computed using the FEYNHIGGS [22] program.

At large values of tanβ, the Higgs boson width increases with $\tan\beta$ and can become significantly larger than the value in the SM. This effect was previously studied by convoluting a relativistic Breit-Wigner function with the next-to-leading order calculation of the signal cross section from FEYNHIGGS as a function of M_ϕ and $\tan\beta$ [8]. In the $(M_A, \tan\beta)$ region where this analysis sets 95% C.L. limits, and for $\mu = +200$ GeV, the Higgs boson width is smaller than $0.1 M_\phi$ and less than half of the experimental resolution on $M_{\rm vis}$. The signal cross section in this channel is largely insensitive to sign(μ). The ratio of the $gg \to \phi$ and $b\bar{b} \to \phi$ cross sections also depends on $\tan\beta$. For this inclusive search, the difference between the efficiencies of the two production mechanisms is small and can be neglected.

The region in the MSSM parameter space excluded at the 95% C.L. is shown in Fig. 3 up to $M_A = 300$ GeV. For $M_A \approx 140$ GeV, the expected exclusion reaches $\tan\beta \approx 30$, which is comparable to recent limits obtained in [6]. The upper limits on the tau pair production cross section for a neutral Higgs boson represent the most stringent

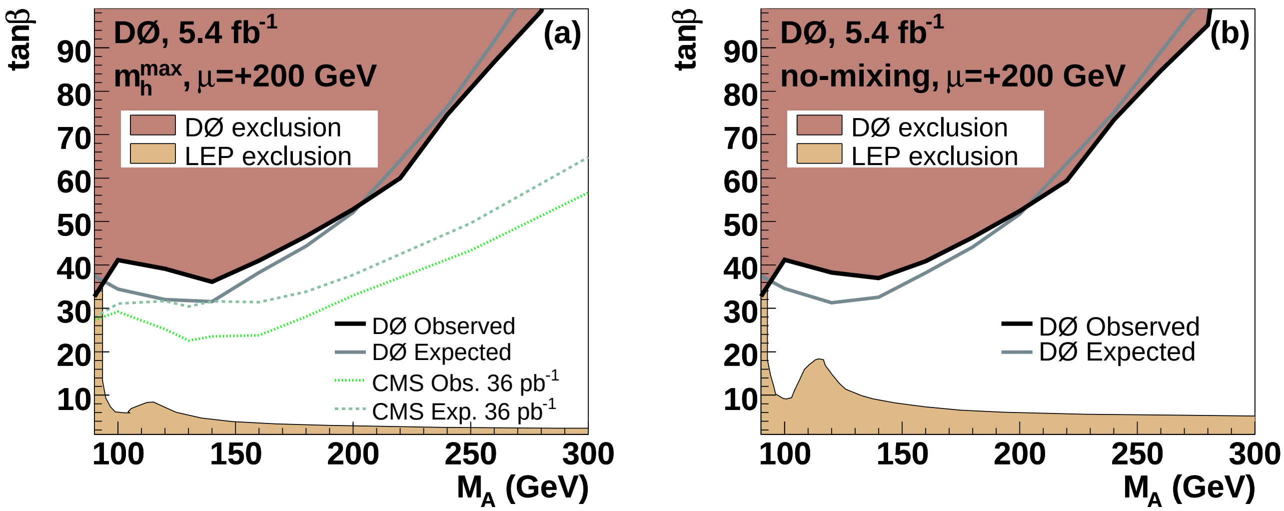

FIG. 3: Expected and observed exclusion regions at the 95% C.L. in the plane of $\tan\beta$ versus M_A for the (a) $m_h^{\rm max}$ and (b) no-mixing scenarios with $\mu = +200$ GeV. The regions excluded by the LEP Collaborations [2] and the CMS Collaboration [6] are also shown.

limits to date at hadron colliders.

We thank the staffs at Fermilab and collaborating institutions, and acknowledge support from the DOE and NSF (USA); CEA and CNRS/IN2P3 (France); FASI, Rosatom and RFBR (Russia); CNPq, FAPERJ, FAPESP and FUNDUNESP (Brazil); DAE and DST (India); Colciencias (Colombia); CONACyT (Mexico); KRF and KOSEF (Korea); CONICET and UBACyT (Argentina); FOM (The Netherlands); STFC and the Royal Society (United Kingdom); MSMT and GACR (Czech Republic); CRC Program and NSERC (Canada); BMBF and DFG (Germany); SFI (Ireland); The Swedish Research Council (Sweden); and CAS and CNSF (China).

---

[1] H. P. Nilles, Phys. Rep. **110**, 1 (1984); H. E. Haber and G. L. Kane, Phys. Rep. **117**, 75 (1985).

[2] S. Schael *et al.* (ALEPH, DELPHI, L3, and OPAL Collaborations), Eur. Phys. J. C **47**, 547 (2006).

[3] T. Affolder *et al.* (CDF Collaboration) Phys. Rev. Lett. **86**, 4472 (2001); V. M. Abazov *et al.* (D0 Collaboration), Phys. Rev. Lett. **95**, 151801 (2005); V. M. Abazov *et al.* (D0 Collaboration), Phys. Rev. Lett. **95**, 221802 (2008); V. M. Abazov *et al.* (D0 Collaboration), Phys. Lett. B **698**, 97 (2011).

[4] V. M. Abazov *et al.* (D0 Collaboration), Phys. Rev. Lett. **102**, 051804 (2009); V. M. Abazov *et al.* (D0 Collaboration), Phys. Rev. Lett. **104**, 151801 (2010).

[5] D. Acosta *et al.* (CDF Collaboration), Phys. Rev. D **72**, 072004 (2005); A. Abulencia *et al.* (CDF Collaboration), Phys. Rev. Lett. **96**, 011802 (2006); V. M. Abazov *et al.* (D0 Collaboration), Phys. Rev. Lett. **97**, 121802 (2006); V. M. Abazov *et al.* (D0 Collaboration), Phys. Rev. Lett. **102**, 051804 (2009).

[6] S. Chatrchyan *et al.* (CMS Collaboration), arXiv:1104.1619, submitted to Phys. Rev. Lett.

[7] T. Aaltonen *et al.* (CDF Collaboration), Phys. Rev. Lett. **103**, 201801 (2009).

[8] V. M. Abazov *et al.* (D0 Collaboration), Phys. Rev. Lett. **101**, 071804 (2008).

[9] V. M. Abazov *et al.* (D0 Collaboration), Nucl. Instrum. Methods Phys. Res. A **565**, 463 (2006).

[10] T. Sjöstrand *et al.*, Comput. Phys. Commun. **135**, 238 (2001).

[11] J. Pumplin *et al.*, J. High Energy Phys. **07**, 012 (2002); D. Stump *et al.*, J. High Energy Phys. **10**, 046 (2003).

[12] M. L. Mangano *et al.*, J. High Energy Phys. **07**, 1 (2003).

[13] Z. Waş, Nucl. Phys. Proc. Suppl. **98**, 96 (2001). We use version 2.5.04.

[14] R. Brun and F. Carminati, CERN Program Library Long Writeup W5013, 1993 (unpublished).

[15] V. M. Abazov *et al.* (D0 Collaboration), Phys. Rev. D **71**, 072004 (2005); Erratum-ibid. D **77** 039901 (2008).

[16] The pseudorapidity is defined as $\eta = -\ln[\tan(\theta/2)]$, where θ is the polar angle with respect to the proton beam direction.

[17] T. Junk, Nucl. Instrum. Methods in Phys. Res. A **434**, 435 (1999); A. Read, J. Phys. G **28**, 2693 (2002).

[18] W. Fisher, FERMILAB-TM-2386-E (2007).

[19] M. S. Carena, S. Heinemeyer, C. E. M. Wagner, and G. Weiglein, Eur. Phys. J. C **26**, 601 (2003).

[20] $M_{\rm SUSY} = 1$ TeV, $X_t = 2$ TeV, $M_2 = 0.2$ TeV, $\mu = +200$ GeV, and $m_{\tilde{g}} = 0.8$ TeV.

[21] $M_{\rm SUSY} = 2$ TeV, $X_t = 0$ TeV, $M_2 = 0.2$ TeV, $\mu = +200$ GeV, and $m_{\tilde{g}} = 1.6$ TeV.

[22] T. Hahn, S. Heinemeyer, W. Hollik, H. Rzehak, and G. Weiglein, Comput. Phys. Commun. **180** 1426 (2009); S. Heinemeyer, W. Hollik, and G. Weiglein, Comput. Phys. Commun. **124**, 76 (2000). We use version 2.8.1.